Active control of the field scattered by the rigid wall of a semi-anechoic room-Simulations and full-scale off-line experiment

C. Pinhède, D. Habault, E. Friot, Ph. Herzog

Active control of the field scattered by the rigid wall of a semi-anechoic room - Simulations and full-scale off-line experiment

C. Pinhède[a,*], D. Habault[a], E. Friot[c], Ph. Herzog[b]

[a] *Aix Marseille Univ, CNRS, Centrale Marseille, LMA UMR 7031, Marseille, France*
[b] *ARTEAC-LAB SAS, 8 allée Léon Gambetta, 13001 Marseille, France*
[c] *13 Bd Rabatau, 13008 Marseille, France*

Abstract

This paper is dedicated to an experimental implementation of active anechoicity control illustrating previous theoretical work. The aim of this experimental is to cancel the pressure scattered by the single rigid wall of a semi-anechoic room, turning the latter into a fully anechoic one over a given frequency range. The proposed method is presented in two steps: estimation of the scattered pressure and its control. Two numerical simulations are presented in order to show the feasibility of the method. An experimental campaign is presented, where the active control system leads to a reduction of the field scattered by the rigid wall throughout a significant part of the measuring volume inside the room. Although these results are based on post-processing of measurements, and not real-time computation, they confirm the possibility to extend the frequency range of a small facility toward lower frequencies, by adding to its passive lining a set of ordinary sources and pressure microphones.

Keywords: Anechoic room, Acoustical measurements, Active noise control, Room acoustics

1. Introduction

Identification of sources may be performed in various acoustical environments, anechoic rooms being the preferred ones for investigating radiation properties. As an example, this is required by the relevant standards for the characterisation of loudspeakers [1, 2]. Most anechoic rooms are however not designed for measurements at the lower audible frequencies, and alternative approaches are required for radiation estimation. In the case of loudspeakers, especially subwoofers, many methods have been proposed (see, *e.g.*, [3–5]) but they may not be considered yet as reliable for measuring any kind of acoustic source. These limitations have motivated investigations about the feasibility to extend the frequency range of existing anechoic rooms toward lower frequencies.

*Corresponding author
Email addresses: pinhede@lma.cnrs-mrs.fr (C. Pinhède), philippe.herzog@arteac-lab.fr (Ph. Herzog)

This extended frequency range may be reached by a hybrid approach, combining the classical absorbing wedges with a set of devices dedicated to the active absorption at lower frequencies. While active absorbers providing local absorption of incident acoustic power have been studied for quite a long time [6–17], the current paper aims at active anechoicity, *i.e.*, cancelling the acoustic 3D field scattered by the walls of the measurement room. Compared with a set of independent active absorbers, the proposed control technique considers the scattered 3D field as a whole and is thus likely to better approximate the desired acoustical environment.

Such a global control of scattered field was first attempted to cancel the exterior field scattered by an object [18–24] and also applied to the interior field scattered by walls surrounding a measured source [25, 26]. In the current paper, the term "scattered field" is used for the pressure equal to the difference between the total pressure (including the walls influence) in the room and the incident pressure (*i.e.*, without walls) emitted by the source. Although it is not fully appropriate in the specific case of the wavefront reflected by a rigid wall, using the term "scattered" emphasizes the similarity with active control of the field scattered by any object subjected to a direct field.

Preliminary work have dealt with the proper design of a hybrid passive/active anechoic room in which the active control was applied to the scattered pressure at any point in the measurement volume of the room [25, 27, 28]. The control sources are located behind the passive wedges and driven from single layer pressure measurements over a closed surface Γ surrounding the measurement volume Ω. The scattered pressure to be cancelled must be first estimated. This is achieved through an off-line calibration step which allows to estimate a matrix relation between the pressure actually measured on Γ and the scattered pressure in Ω. An analysis of the existence and uniqueness of the underlying operator involved in this relation is given in Ref. [28], confirming the validity of this approach which was previously tested on a small-scale mock-up [27].

The present paper deals with an experimental validation of the active anechoicity concept on a full-scale facility. Such an experiment leads to several kinds of practical difficulties discussed in the next sections. To reduce the burden associated with a set-up involving a large number of channels, this first experiment was conducted in a semi-anechoic room available in our laboratory for a sufficient period of time. In this room, five walls are expected to be absorbing. Therefore the active set-up was used to ensure absorption over the single remaining hard surface [29] and the surface Γ was defined as a finite-dimension grid parallel to this surface (see Fig. 1). This semi-anechoic configuration seemed an adequate intermediate step before tackling the equipment of a fully anechoic room.

Numerical simulations were first performed in order to prepare the experiment and assess the validity of the chosen configuration. Secondly, the data collected in the experiments was post-processed in order to simulate off-line active control: the total pressure without control at the microphones and the measured transfer paths from the control sources to the microphones allowed the computation of control signals whose effect on the microphones was simulated through linear superposition. Due to time constraints, no attempt was made at implementing real-time control in this case involving a large number of channels.

Section 2 recalls the two-step method (calibration and control) developed here following in Ref. [28]. Section 3

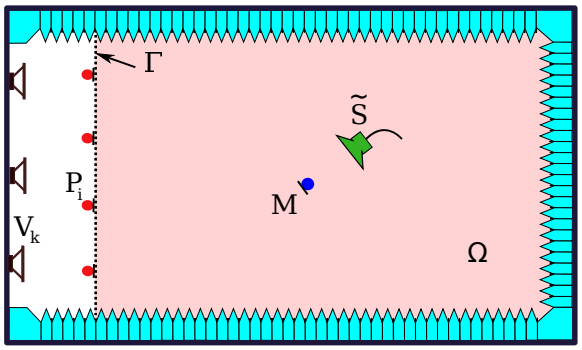

Figure 1: Scheme of an active control in the semi-anechoic room.

describes the geometry of the semi-anechoic room, the configurations used for both numerical and experimental studies and the numerical test on the efficiency of the identification step. Section 4 gives the details of the experimental procedure. Section 5 presents some of the experimental results.

2. Reminder of the theoretical basis

The approach follows the one described in Ref. [28]. It consists in driving control (also called secondary) sources so as to cancel out the scattered pressure when a primary source $\tilde{S}$ is being measured inside the semi-anechoic room (Fig. 1). This is achieved through an adaptive process similar to active noise control, where the pressure to be minimised is the pressure scattered by the walls into volume Ω.

2.1. Strategy for a global control

Accounting for the anechoicity of five walls, the test-case studied here is similar to the half-space case of Ref. [28] except for the fact that the reflecting wall has a finite size. This geometry has been considered as suitable for a first practical implementation to check the validity of the method in a realistic situation.

The placement of the control sources and microphones is a major concern. Since the scattered field is due to the rigid wall, placing the control sources V_k on this wall seems to be optimum. Moreover, this is compatible with its expected use in an anechoic room, especially if the sources are hidden behind its passive lining. For the positions of the control microphones, the choice is far less obvious. In Ref. [28], control of the scattered field was only simulated at a few locations inside the measurement volume Ω but a practical use would require to ensure a significant reduction of the scattered field throughout a part of Ω as large as possible. Within a limited frequency band, such a control could be achieved by using an even distribution of control microphones inside Ω. This would however not be convenient as these microphones need to remain inside the room during further experiments using active control. Improving the control efficiency would lead to increasing the number of control microphones within the measuring volume, and their supporting structures would restrict the usefulness of the facility and possibly bias the measurements. Moreover,

spreading control microphones throughout the volume leads to a wide range of distances from the reflection sources, possibly leading to low values of signal-to-noise ratio and a bad conditioning of the matrix used in the computation of the control commands.

Another configuration was therefore considered, with control sensors distributed over the surface Γ itself. Although such a choice does not fully satisfy the mathematical requirements of Ref. [28], it was tested because of its many advantages. First, it keeps clear the measuring volume. Secondly, microphones closer to the reflecting wall provide a better sensing of the scattered field (which is maximum near the wall). Thirdly, the transfer matrix from the control sources to a cluster of microphones has generally a better conditioning when the cluster is close to the sources. Such a matrix leads to lower source level and better convergence of real-time control algorithms (see Ref. [30]). Finally, microphones on Γ do not interfere with setting-up and conducting experiments in the room. Using a large number of fixed microphones covering all the scattering surface then leads to an overdetermined global control problem. No regularisation is required in the computation of optimal control and, because global control is aimed at, the whole process of computing the error signals and the control signals is probably more robust than when trying to reduce the scattered pressure at a small set of microphones inside the room.

2.2. Step 1 - Estimation of the scattered pressure

The main difficulty of the method is that the scattered pressure to be minimised cannot be directly measured. While it could be estimated from directive sensors or dual-layer pressure measurements, our choice is to process single-layer pressure measurements as this involves less numerous and simpler sensors. This adds a preliminary step in the process, hereafter called "identification step", during which the scattered pressure is assessed at a point of Ω by processing single-layer measurements of the total pressure on the surface Γ. Indeed it was shown in Ref. [28] that there exists a scattering operator $\mathcal{H}$ which, for any source S, relates the scattered pressure $p_{\text{sca}}(S, M \in \Omega)$ to the total pressures $p_{\text{tot}}(S, P \in \Gamma)$:

$$p_{\text{sca}}(S, M) = \int_{\Gamma} p_{\text{tot}}(S, P)\mathcal{H}(M, P)d\Gamma(P). \tag{1}$$

Details about this operator and some of its properties are given in Ref. [28], however $\mathcal{H}$ is not explicitly known. For practical purposes, its estimation is obtained through a discretisation of the integral in Eq. (1) and a series of preliminary off-line measurements. The unknown is then a vector of "filters" $\hat{\mathbf{H}}(M, P_i)$ which relates the scattered pressure at one point M to the estimation of total pressures at a set of discrete N_m locations P_i of Γ. The identification of the filters is based upon the use of a "reference source", *i.e.*, a source with a know radiation pattern. Indeed, since $\mathcal{H}$ does not depend on the source, $\hat{\mathbf{H}}$ can be estimated by minimising a cost function $F(S_j, M)$ by solving a linear system for a set of measurements at N positions S_j of the reference source:

$$F(S_j, M) = \left\| p_{\text{sca}}(S_j, M) - \sum_{i=1}^{N_m} p_{\text{tot}}(S_j, P_i)\hat{\mathbf{H}}(M, P_i) \right\|^2 + \lambda \left\| \hat{\mathbf{H}} \right\|^2. \tag{2}$$

The values $p_{\text{sca}}(S_j, M)$ are obtained from:

$$p_{\text{sca}}(S_j, M) = p_{\text{tot}}(S_j, M) - p_{\text{inc}}(S_j, M), \tag{3}$$

where the total pressure p_{tot} is measured at point M and the incident pressure p_{inc} is deduced from the known radiation pattern of the reference source. The second term on the right-hand side constrains the norm of $\hat{\mathbf{H}}$ in order to regularise the inverse problem. With a number of sources significantly larger than the number of microphones, and provided that the condition number of the matrix problem is not too high, the cost parameter λ may be set to a very low value or even to zero. In the case of active control, the point M represents one of the control points where the scattered pressure must be minimised. As said previously, it is decided here to locate these points on Γ and furthermore the same set of points P_i are chosen as both the identification and control points. The whole procedure of identification can be summarized as follows:

1. A reference source with known radiation pattern is selected (see section 4.2).
2. The number and positions of the source S_j and points P_i are chosen. The number of S_j is chosen to be larger than the number of P_i leading to an overdetermined identification problem.
3. The values of $p_{\text{inc}}(S_j, P_i)$ are computed from the known radiation of S; during the experiment the amplitude of the source is measured by a microphone located inside the source (see section 4.2).
4. The values of $p_{\text{tot}}(S_j, P_i)$ are directly measured in the semi-anechoic room and used to assess the values of $p_{\text{sca}}(S_j, P_i)$ from Eq. (3).
5. Assuming a suitable discretisation, matrix $\mathbf{H}$ may be defined by

   $$\mathbf{H}_{ni} = \mathcal{H}(P_n, P_i) \text{ for n and } i = 1, \ldots, N_m$$

   which is approximated by minimising the system $F(S_j, P_n)$ for $j = 1$ to N and $n = 1$ to N_m. The filter matrix $\mathbf{H}$ is composed of n vectors filters $\hat{\mathbf{H}}$:

   $$\mathbf{H}_{ni} = \hat{\mathbf{H}}(P_n, P_i).$$

The proposed method depends on the adequate identification of the filter matrix $\mathbf{H}$. Although the parametric study of this identification technique is beyond the scope of the present paper, Fig. 2 illustrates the accuracy of this estimation, for simulations using 24 and 32 source positions, assessed from the error on the scattered pressure, averaged on the 16 control points. Two comparisons are shown for 24 and 32 positions of the reference source. Using 24 sources, this error is already relatively low (less than 2 dB) over the frequency band of interest. It is only marginally reduced when increasing the number of source positions to 32, suggesting that the method has almost converged. The experiment was hereafter conducted using 32 sources positions.

2.3. Step 2 - Active control of the scattered pressure

Once the scattered pressure resulting from the primary source has been estimated, it can be minimised using standard active control. As previously mentionned, the control points are the points P_n on Γ. The active control of the

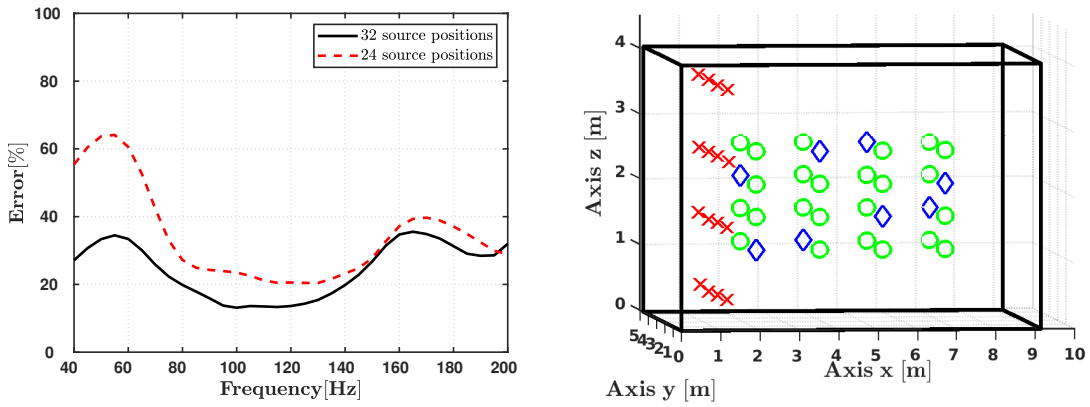

(a) (b)

Figure 2: (a) Relative error between direct simulation and estimation of the scattered field, averaged over 16 microphone positions, for 24 and 32 reference source positions. (b) Microphone positions (×); 24 first source positions (○), 8 additional source positions (◊).

scattered pressure at the positions P_n is based on the estimation of the control commands $\mathbf{u}$ of a set of N_k secondary sources V_k, obtained by minimising the quantity:

$$J(P_n) = \left\| p^a_{\text{sca}}(\tilde{S}, P_n) + \sum_{k=1}^{N_k} \mathbf{C_t}(V_k, P_n) u(V_k) \right\|^2 + \alpha \ \|\mathbf{u}\|^2 , \tag{4}$$

where the scattered pressure $p^a_{\text{sca}}(\tilde{S}, P_n)$ due to $\tilde{S}$ at point P_n is estimated through the matrix $\mathbf{H}$ obtained at the previous step:

$$p^a_{\text{sca}}(\tilde{S}, P_n) = \sum_{i=1}^{N_m} p_{\text{tot}}(\tilde{S}, P_j) \mathbf{H}(P_n, P_i). \tag{5}$$

The elements $\mathbf{C_t}(V_k, P_n)$ of the $\mathbf{C_t}$ matrix are the transfer functions between the command of V_k secondary sources and the resulting pressure at P_n points. The control commands $\mathbf{u}$ are then obtained as the solution of the regularised minimisation problem with a cost parameter α limiting the output level of the control sources. This parameter α can also help to determine the appropriate leakage parameter of an FxLMS algorithm in real-time implementation [31]. However when there are more microphones than secondary sources, as in the present study, the control problem is overdetermined and α may theoretically be set to a very low value or even to zero in Eq. (4).

3. Test case and preliminary simulations

Preliminary simulations have been conducted in order to check the validity of the configuration intended for the experiment. The geometry used for the simulation is as close as possible to the experimental one, however the acoustic boundary conditions are only roughly approximated: the aim of these simulations is to check the adequateness of the configuration, they are not intended for a quantitative comparison with experimental results.

3.1. Geometry and simulation conditions

One side wall is made of concrete, with an opening covered by a heavy and stiff plate, so that it is assumed to be an almost perfectly reflecting surface. The dimensions of the room are $L_x = 9.15$ m, $L_y = 4.6$ m and $L_z = 4.05$ m. Fig. 3 shows horizontal and vertical views of the problem geometry (see also Fig. 5 and 6).

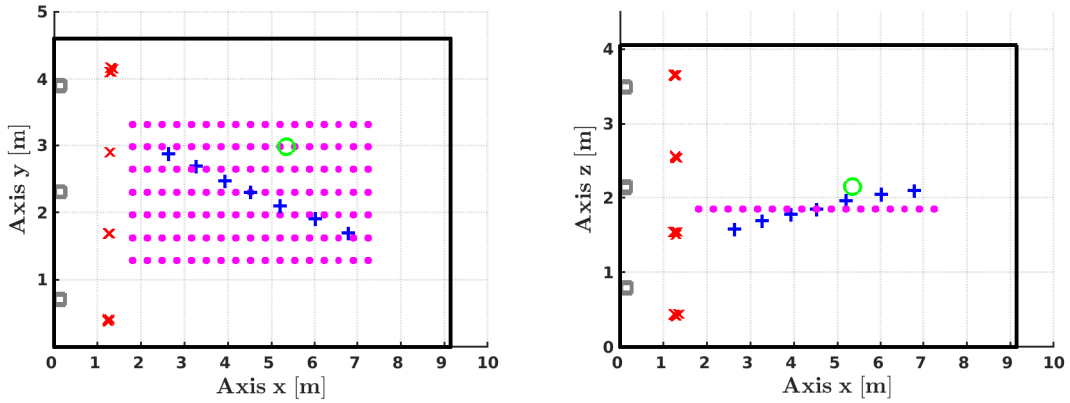

(a) (b)

Figure 3: Geometry for simulations - source $\tilde{S}$ (◯), secondary sources V_k (□), identification and control microphones P_Γ (×), observation microphones Q_{Plane} (•), observation microphones Q_{Line} (+).

The computations are carried out in the [40 − 200] Hz frequency band. Therefore the maximum dimension of the room is of the order of 1 to 5.4 wavelengths. For the simulations, the walls are considered as plane and their acoustic behaviour is described by a localised boundary condition . The reflecting wall is described by a tiny complex admittance $\beta = 10^{-3}(1 + i)$ and the five absorbing walls by the characteristic specific admittance, *i.e.*, $\beta = 1$. These values are uniform on each wall and kept constant over the whole frequency band. Such a coarse representation does not allow a comparison between the simulated and measured pressures. It is however assumed that such simulations would provide the main trends of the behaviour of various active control set-ups.

Three sets of microphones are used. The set P_Γ includes 16 microphones P_i located on Γ and used as identification and control microphones. Here, Γ is a vertical grid, located 1.3 m away from the reflecting wall. The P_Γ microphones are regularly spaced, in a rectangular array made of 4 vertical lines, each one with 4 microphones. Table 1 gives the positions of these vertical and horizontal lines of the grid. The mean interval between two microphones is 1.2 m (corresponding to a half wavelength at 130 Hz).

The sets Q_{Line} and Q_{Plane} correspond to observation microphones located within the volume Ω and used to check the efficiency of the control. The distances $d_w(\Gamma, Q_{\text{Line}})$ and $d_s(\tilde{S}, Q_{\text{Line}})$ of the 7 points of Q_{Line} to the surface Γ and to the primary source $\tilde{S}$ are reported in Table 2. The 119 points of Q_{Plane} are equally spaced, belonging to a plane horizontal array defined by 1.8 m $\leq x \leq$ 7.2 m; 1.2 m $\leq y \leq$ 3.3 m; $z = 1.8$ m.

y	0.4	1.69	2.9	4.15
z	0.44	1.54	2.54	3.65

Table 1: Horizontal and vertical coordinates (in meters) of the identification microphones P_Γ.

Microphones	Q_1	Q_2	Q_3	Q_4	Q_5	Q_6	Q_7
$d_w(\Gamma, Q_j)$	1.33	1.96	2.64	3.22	3.90	4.71	5.50
$d_s(\tilde{S}, Q_j)$	2.77	2.15	1.55	1.11	0.91	1.26	1.93

Table 2: Distances d_w and d_s in meters.

In the simulations, all sources are assumed to be ideal monopole sources with prescribed volume velocity. Their positions are supposed to match the acoustic centres of the actual sources used for the experiment. The primary source $\tilde{S}$ is located at coordinates (x = 5.3 m, y = 3.0 m, z = 2.1 m). The 32 positions S_j of the reference source are regularly spaced inside a rectangular volume (their locations are given in Table 3). The 9 control sources V_k are all placed in a plane parallel to the wall at a mean distance of x = 0.15 m and 3 heights z = 0.8 m; 2.1 m; 3.5 m. The mean interval between adjacent sources is 1.5 m (*i.e.*, a half wavelength at 170 Hz).

x	2.14	3.76	5.36	7.0
y	1.2	3.27		
z	1.14	1.64	2.14	2.64

Table 3: Coordinates (in meters) which 32 combinations define the S_j sources positions.

3.2. Simulation of the identification step

Several series of numerical simulations were conducted using a custom software (named FELIN) based on the Boundary Element Method (BEM). It was chosen for convenience but any other code and/or method (*e.g.*, Finite Element Method) could be used as well.

In order to point out the effect of the identification step on the control, two cases of control are presented here. In both cases the commands are obtained from Eq. (4). In Sec. 3.2.1, the p^a_{sca} term is taken as the exact scattered pressure computed using the BEM software while for simulations presented in Sec. 3.2.2 the p^a_{sca} values are obtained from the estimation of $\mathbf{H}$, as in a real case.

Levels (in dB) obtained at frequencies 95 and 125 Hz are shown as color maps in Fig. 4 with and without control of the scattered pressure. On each map and at each point, the levels represent the difference in levels between the

total pressure and the incident pressure, for the point source $\tilde{S}$. The coloured lines map the results in Q_{Plane}. The coloured diamonds numbered from 1 to 7 correspond to Q_{Line} and are superimposed over the map (although they are not in the Q_{Plane} plane). Without control, the map illustrates the effect of the boundaries. With control on, the map emphasizes the efficiency of the control. The colors are green when the scattered pressure is small or efficiently controlled (within ±1.5 dB). On the left-hand side of each map, the vertical line featuring four diamonds indicates the levels computed at each of the identification microphones P_Γ. Each diamond, divided into 4 parts, corresponds to a column of 4 microphones.

3.2.1. Control using the exact scattered pressure

When performing simulations, it is possible to control the scattered pressure (as computed by the BEM code) instead of its estimation through the **H** filter matrix. Fig. 4 shows levels obtained at 95 (left) and 125 Hz (right) without control (upper row) and with control using the exact scattered pressure (second row).

All these maps show significant differences between the incident and total pressures close to the reflecting wall. Without control, these differences are observed over a large part of the measuring area, especially at 125 Hz. With control on, a large part of the observation points shows acceptable discrepancies (visible as a wider green area). The best results are obtained at 125 Hz for which the control is efficient for most of the abscissas above 2.3 m. These results show that the control does lead to correct results on Q_{Line} and Q_{Plane}.

3.2.2. Control with the estimated scattered pressure

For the next simulations, the control is used to minimise the pressure p^a_{sca} estimated through the filter matrix **H** mimicking what would be done in an experimental situation. The preliminary identification of **H** is conducted with the 32 S_j positions of a reference source and the same P_Γ set of 16 identification microphones. The commands are then obtained from Eq. (4) where the points of P_Γ are also used as the control microphones. For practical implementation purposes, cost parameters λ in Eq. (2) and α in Eq. (4) were not set to zero but to 10^{-16}, which is the smallest non-zero number in the computer.

The lower row of Fig. 4 shows the total sound pressure obtained with the control commands computed using the estimated scattered pressure. The results are quite similar to those obtained with the exact scattered pressure. Some comparisons not presented here were also carried out for various numbers of control points inside the volume Ω. They confirmed the simulations presented in previous works [27, 28], showing that both types of control (inside Ω or over Γ) lead to similar results.

The above simulations also suggest that the estimation of the scattering operator is not required with an accuracy higher than the one obtained from the simple approach exposed here. This is a good point as such a configuration leads to a relatively simple experimental set-up. It also tends to validate the control of scattering using a single layer

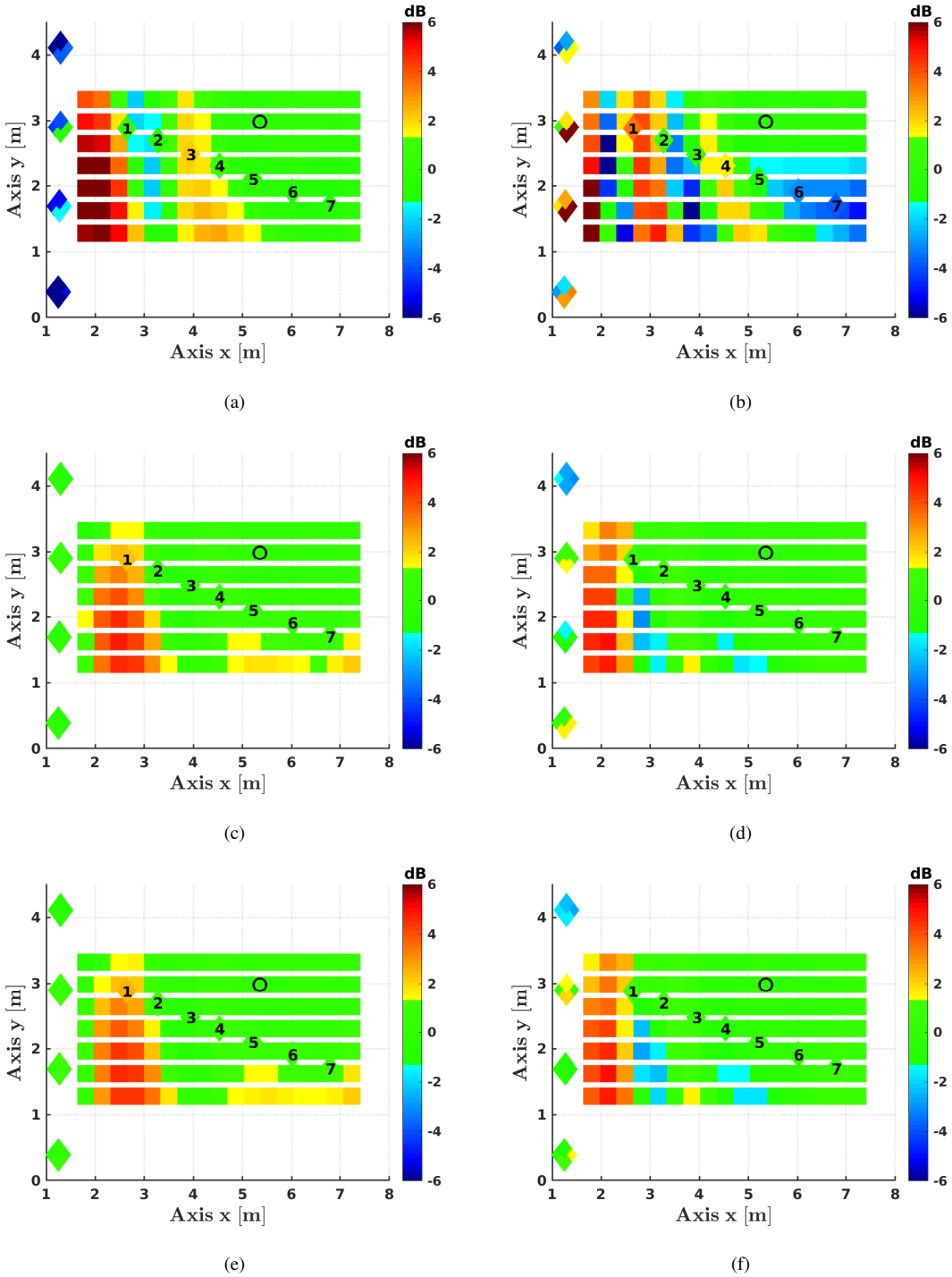

Figure 4: Control observed on Q_{Line} and Q_{Plane} at 95 Hz (a,c,e) and 125 Hz (b,d,f). Control off (a,b), control of simulated scattered pressure (c,d) and control of estimated scattered pressure (e,f).

of pressure measurements on Γ.

4. Experimental procedure

The experimental set-up features two sets of microphones: P_Γ for the identification and control steps and Q_{Line} used to check the control efficiency. The corresponding geometry is presented in Fig. 5 in a (O, x, y, z) cartesian coordinate system. The z axis is vertical and the vertical reflecting wall corresponds to the plane $x = 0$.

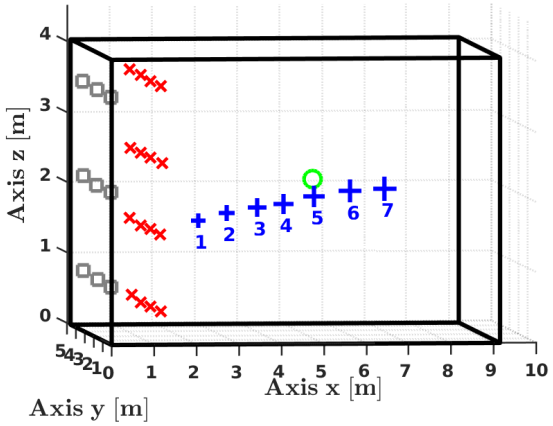

Figure 5: 3D scheme of the experiment - source $\tilde{S}$ (◯), secondary sources V_k (□), identification microphones P_Γ (×), observation microphones Q_{Line} (+).

A partial view of the semi-anechoic room is shown in Fig. 6. The source on the right is the primary source $\tilde{S}$ (*cf* section 4.2). The secondary sources on the rigid wall may be seen on the left part of the picture. The crosses (× and +) respectively indicate the positions of the P_Γ and Q_{Line} microphones.

4.1. Equipment

For the control step, 9 loudspeakers V_k were mounted close to the vertical rigid wall. They were active compact sub-woofers, each one featuring two 8-inch loudspeakers in a push-pull configuration. Their internal circuits have been modified, resulting in an effective frequency range of $[40 - 200]$ Hz. The total volume of each source was 0.05 m^3. The acoustic centre, assumed to be the geometric centre of the two loudspeakers, was located at 0.15 m from the wall.

The 23 pressure sensors used for P_Γ and Q_{Line} were 1/4-inch electrets microphones (CTTM MK90) connected to their conditioning amplifiers (CTTM Pre_MK).

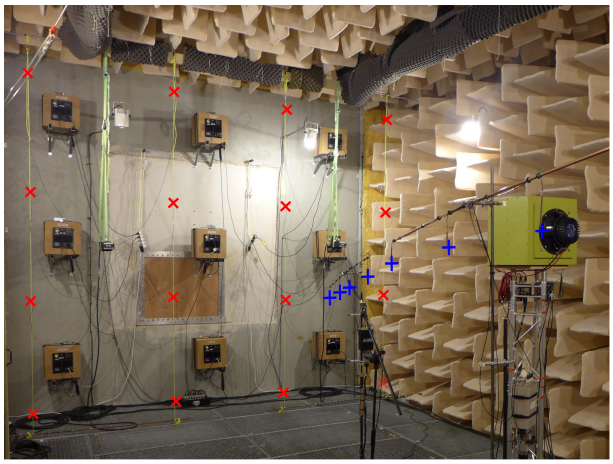

Figure 6: A partial view of the semi-anechoic room.

The acquisition/restitution system was based upon an Audio RME HDSP Madi card and Sonic Core AD/DA and RME ADI-468 Madi/ADAT converters. The sampling frequency was 44.1 kHz. A custom software program was used to play a multichannel WAV file on the output while simultaneously recording the input data to another WAV file.

The signals used during measurements were sine signals swept over the [40 – 400] Hz frequency band, following the method described in Ref. [32].

4.2. Reference source

In the previous simulations, the radiation pattern of the reference source was assumed to be perfectly known and monopolar - which is not fully realistic. A "reference source" had been previously designed in order to be able to radiate a pre-defined pressure field, as required for the identification step of the method. The design and model of this source are fully described in Ref. [33] and briefly presented here.

For the sake of simplicity, this source has been targeted to be as close as possible to an omnidirectional compact one, at least at low frequencies. It has therefore been built using two 10-inch speakers (BEYMA 10LW30/N) facing each other, mounted on an almost cubic closed box of $V_s = 42.4\ \ell$ internal volume. A high-pressure microphone (GRAS 40BF) is located inside the closed volume, close to its centre. This microphone provides a measurement p_{int} of the internal acoustic pressure which is assumed to be proportional to the speaker membrane displacements (as the isobaric mode should be dominant inside such a compact closed box). This measurement is thus used as a reference to estimate the source volume velocity and then the pressure that would be radiated by the source in free field. As explained in Ref. [33], the model required to obtain a correct estimation p_{mod} of the free-field pressure (direct sound) features two monopoles, S_{r1} and S_{r2} (one for each speaker, with identical volume velocities and phases). The positions of these monopoles were deduced from geometrical measurements, their distance was estimated as 0.6 m, with locations symmetric with respect to the source centre. The p_{mod} pressure is thus related to the internal pressure

p_{int} by the following equation:

$$p_{\text{mod}}(P) = p_{\text{int}} \frac{\omega^2 V_s}{c^2} \{ \frac{e^{-\imath kr(S_{r1},P)}}{8\pi r(S_{r1},P)} + \frac{e^{-\imath kr(S_{r2},P)}}{8\pi r(S_{r2},P)} \} \tag{6}$$

where ω, ρ and c are respectively the angular frequency of the signal, the air density and the sound velocity in air, respectively.

The distance between the two monopoles is not significant below 120 Hz (where the source behaves like a monopole source) but the two-monopole model is required at higher frequencies.

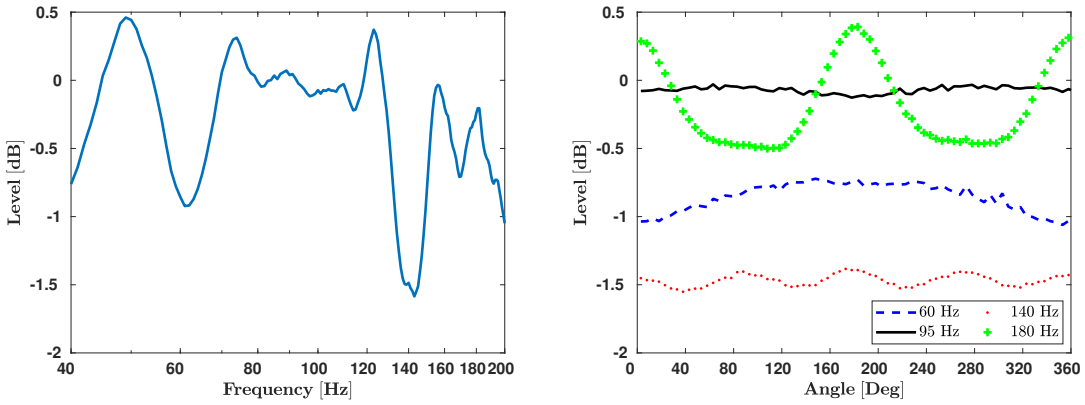

(a) (b)

Figure 7: The *Err* function (levels in dB) (a) as a function of frequency (average on all angles), (b) as a function of angle, for 4 frequencies.

The radiation model proposed above has been validated with measurements performed in a large anechoic room, over a circle of radius 1.04 m in a horizontal plane. Fig. 7 shows the amplitude of the relative error $Err = p_{\text{meas}}/p_{\text{mod}}$ between the measured pressure p_{meas} and the pressure p_{mod} computed from the above model. First, Fig. 7(a) shows the behaviour of Err as a function of frequency. The curve shows for each frequency the value of Err averaged over all incidence angles and expressed in levels (dB). It remains within $[-0.5; 0.5]$ dB in the frequency bands $[70 - 130]$ and $[150 - 180]$ Hz. Below 70 Hz (room cut-off frequency) the room is not anechoic and between 130 and 150 Hz, it presents some resonance phenomena as already stated in Ref. [34].

More details are given in Fig. 7(b) which shows Err as a function of the incident angle, for some frequencies. At 60 and 140 Hz, the error has weak angular variations, but is larger than 0.5 dB. At 180 Hz, it even oscillates between -0.5 and 0.5 dB. Conversely the error curve is smooth and close to 0 dB at 95 Hz and other measurements not shown here indicate that the two-monopole model provides a good description of the source radiation between 70 and 130 Hz.

For practical reasons, the same source is used at the S_j set of positions for the identification step, in order to identify the filter matrix $\mathbf{H}$, and also as the "unknown" source $\tilde{S}$ to be characterised. This is a way to quantify the

performance of the active scattering control. Further work will have to deal with other kinds of sources with more complex radiation patterns.

4.3. Semi-anechoic room

The room used for the experiment is a semi-anechoic room featuring five absorbing walls, covered with rockwool wedges protected by fabric housing. They are supposed to ensure a 80 Hz cut-off frequency, however the acoustical behaviour of the room is modified by the presence of a supporting metallic grating which was left for practical reasons.

The acoustical environment was therefore assessed at points Q_{Line}, before attempting active control of the scattered pressure. Fig. 8 shows a comparison between measured and computed sound pressures at the four observation points Q_1, Q_3, Q_5 and Q_7. For each location, the solid curve is the measured pressure. The other curves are computed using the internal pressure inside the source and the model of the reference source (Eq. (6)), assuming two different boundary conditions: the dotted curve is computed assuming an infinite rigid plane, while the dashed one is computed using the BEM software and the impedance values given in Sec. 3.

The curves of Fig. 8 correspond to the ratio (expressed in dB) between the measured or computed pressure and the pressure computed with the source model in free space. The 0-dB value should thus correspond to a fully anechoic situation and deviations from 0 dB illustrate the effect of the actual boundary conditions.

All measurements below 75 Hz are quite different from the two models. The room seems to have a modal behaviour, leading to a minimum pressure around 45 Hz and a maximum pressure around 58 Hz. As expected from the stated cut-off frequency, the five walls fitted with acoustic lining cannot be considered as significantly absorbing at such low frequencies.

Above 80 Hz, the three curves show interference patterns, with similar positions of minima and maxima. The measured curve lies usually between the two simulated ones. The dominant boundary effect thus seems to be related to the reflection on the rigid wall. Its effect also depends on the measured point and is smaller for point Q_5 (the point closest to the source).

At point Q_7, further from the reflecting wall and the source and closer to the absorbing walls, the measured curve significantly differs from the infinite plane simulation. The BEM simulations cannot fully take into account the acoustical behaviour of the wedges (using a simple admittance boundary condition). They seem however closer to the measurements, probably because the room lining cannot be considered as perfectly absorbing neither.

4.4. Experimental processing

The identification step was conducted with 32 positions S_j. The total pressures $p_{\text{tot}}(S_j, P_n)$ were directly measured. The scattered ones $p_{\text{sca}}(S_j, P_n)$ were deduced from Eq. (3), where $p_{\text{inc}}(S_j, P_n)$ was estimated from the measurement of the reference pressure at the microphone placed inside the source, following Eq. (6). The set-up was controlled using a laser theodolite allowing precise recording of the relative positions of each object: the accuracy of

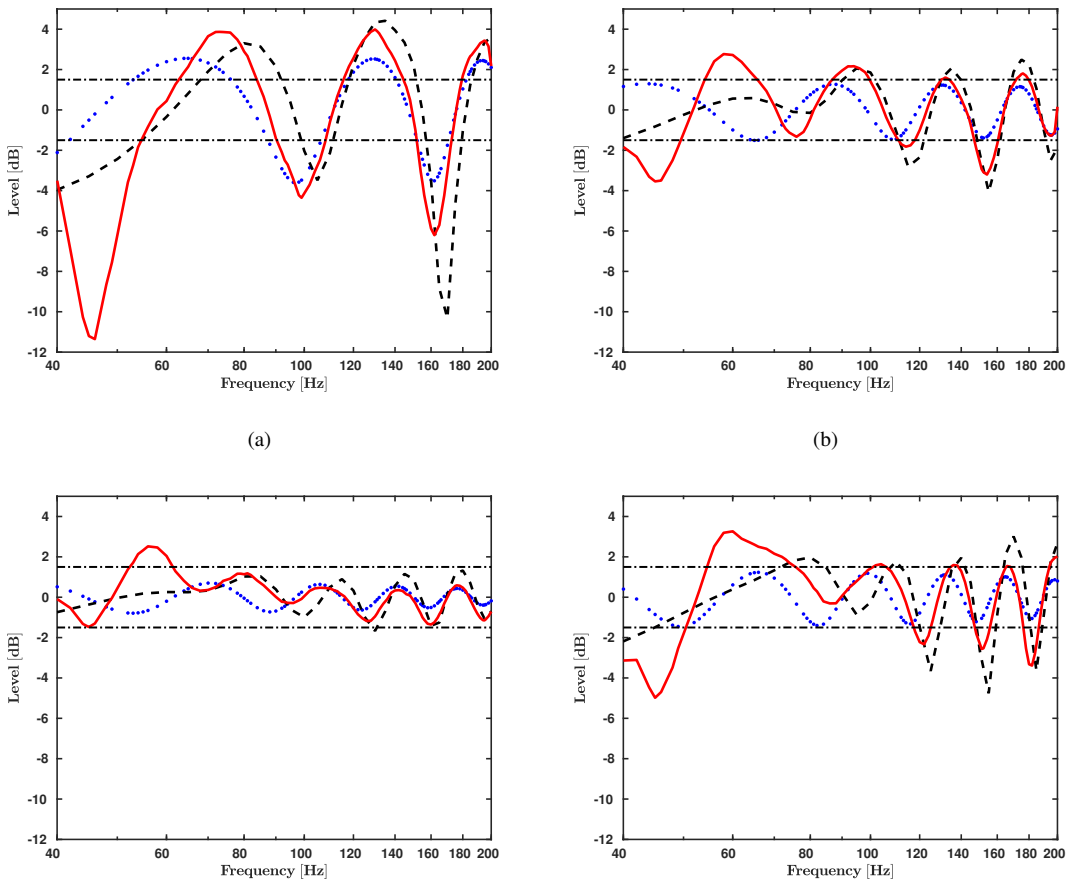

Figure 8: Sound pressure levels measured (——) and computed (infinite rigid wall • • • •; Felin — —) at 4 points. (a) Q_1, (b) Q_3, (c) Q_5, (d) Q_7.

distances r in Eq. (6) is therefore of the order of one centimeter. The filter matrix $\mathbf{H}$ was then obtained as the solution of the minimisation problem defined by Eq. (2).

For the control step, the transfer function matrix $\mathbf{C_t}(V_k, P_n)$ was first measured. Then the total pressures $p_{\text{tot}}(\tilde{S}, P_n)$ were measured in order to compute the scattered pressures $p^a_{\text{sca}}(\tilde{S}, P_n)$ using Eq. (5). Finally the source commands $u(V_k)$ were obtained by minimising the cost function J at the locations P_Γ, following Eq. (4).

As discussed before, real-time control was not implemented for this experiment. The controlled pressure was therefore estimated by using the following relation:

$$p^e_{\text{on}}(\tilde{S}, Q_\ell) = p_{\text{tot}}(\tilde{S}, Q_\ell) + \sum_{k=1}^{9} \mathbf{C_t}(V_k, Q_\ell) u(V_k) \tag{7}$$

where p_{tot} is the total pressure measured without control.

Although the controlled pressure was not obtained from a direct measurement, this linear combination of experimental results is considered to give a reliable estimate provided the sources are linear enough at the considered drive levels, which was checked through distorsion measurements (not shown here).

5. Experimental results

Fig. 9 shows the total pressures $p_{\text{tot}}(\tilde{S}, Q_{\text{Line}})$ measured with and without control. They are presented similarly as in Fig. 8. In each figure, the dotted line corresponds to the total pressure measured without control. The solid line is the total pressure with control, computed from Eq. (7).

These first experimental results deserve many comments, the main ones being summarised here:

- Except for the microphone closest to the reflecting wall (Fig. 9(a)), the control has almost no effect below 75 Hz. Below the room cut-off frequency, significant reflections take place on all the walls and the room response is dominated by acoustic modes. Reducing the pressure scattered by a single wall cannot have a large effect when the scattering by the other walls is also significant. It is therefore not a surprise that control has no effect at these low frequencies.

- The best control results are obtained at locations Q_2 to Q_6, for frequencies between 75 Hz and 180 Hz. This upper frequency limit is somewhat higher than expected, considering the microphone spacing of the P_Γ set. It may result from the relatively simple field incident on the rigid wall from the $\tilde{S}$ source (almost planar wavefront considering its distance).

- Results are still very good over the whole [80 – 200] Hz frequency band at Q_7. Without control, the pressure at Q_7 shows a larger interference pattern than at Q_6 - which suggests that the pressure scattered by the non-rigid walls becomes significant - however the scattering control over the rigid wall seems to have a significant effect at Q_7. This has to be further investigated.

- Measurement point Q_1 is close to the rigid wall, but not so close to the source. The control allows to reduce the scattered field, resulting to an error below 1.5 dB over the [80 – 140] Hz frequency band. This frequency band is the one for which the control is expected to be efficient, but its performance is somewhat disappointing compared with other locations: although the scattered field has a maximum value at this location, it does not seem to be controlled efficiently.

In summary this first experiment tends to validate the active control of scattering over the P_Γ set of microphones, using an experimental estimate $\mathbf{H}$ of the $\mathcal{H}$ scattering operator. However, it seems to control part of the pressure scattered by the non-rigid walls, while it does not seem to control as efficiently the scattered field for points close to the rigid wall.

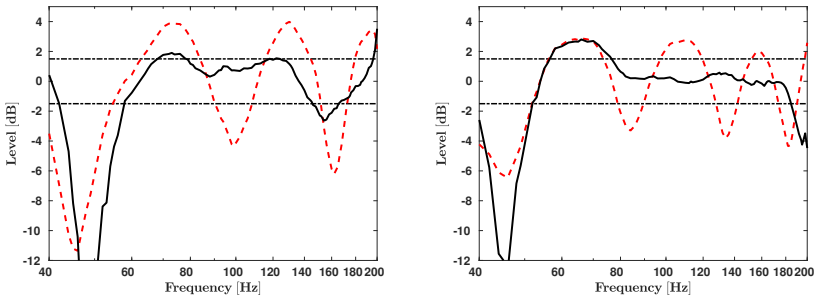

(a)

(b)

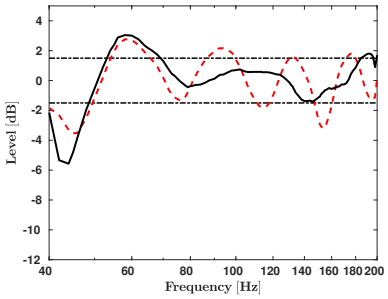

(c)

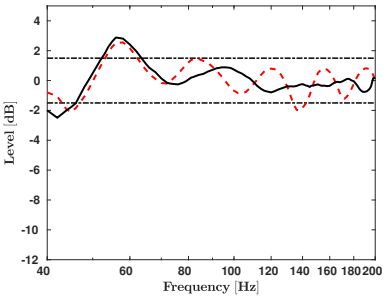

(d)

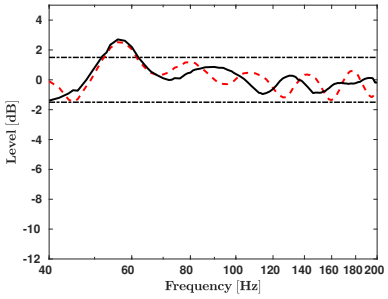

(e)

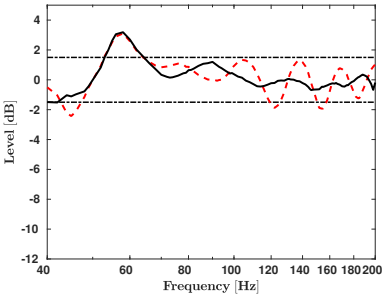

(f)

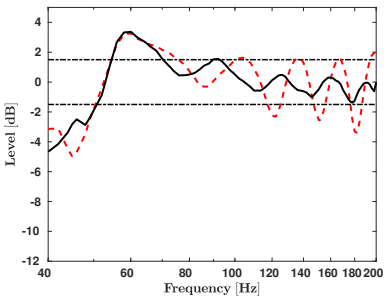

(g)

Figure 9: Control on P_Γ observed on Q_{Line}. Control off (– – –), Control on (———). (a) Q_1, (b) Q_2, (c) Q_3, (d) Q_4, (e) Q_5, (f) Q_6, (g) Q_7.

The fact that some control may be achieved at Q_7 may result from the incorrect estimation of the filter matrix $\mathbf{H}$. As shown by Fig. 2, the accuracy of its estimation is degraded below 80 Hz, even close to the rigid wall. As the radiation model of the reference source is supposed to be better at lower frequencies, it is likely that the contribution of the 5 other walls becomes quite significant at lower frequencies. The system thus identifies filters including the contributions of all the walls instead of the single rigid one, and the system therefore attempts to minimise this combined error signal.

The deceiving control results at Q_1 may result from the system geometry: the system builds a secondary pressure field which is supposed to cancel out the pressure scattered by the rigid wall, using control sources which are separated from each other by about 1.5 m. The discrete sum of the control source contributions cannot build an arbitrary wavefront at ranges shorter or comparable to this spacing. The secondary wavefront at Q_1, and to some extent at Q_2, is therefore probably less accurate than further away from the control sources.

Moreover, numerical simulations suggest that the acoustic field exhibit rapid spatial changes near the wall. The estimation of the scattered pressure might then be more sensitive to measurement errors or variations of the sound speed.

6. Conclusion

This work has investigated the experimental feasibility of an active control of the pressure scattered by the rigid wall of a semi-anechoic room, in order to achieve full anechoicity. As in previous publications [27, 28], the method considered here is to drive sources located over the rigid wall from a single layer of pressure sensors close to this wall. This requires the off-line identification of a filter matrix relating the total pressure to the scattered pressure, approximating the underlying operator. Numerical simulations have led to encouraging results, even with the simplest set-up considered. A first experiment was designed and allowed to reduce significantly the scattered pressure, over frequencies ranging from the cut-off of the semi-anechoic room to an upper limit related to the source and microphone density over the rigid wall.

Simulations showed that the off-line estimation of the scattering operator leads to control performances very close to the use of theoretical values. This suggests that its estimation is not as critical as previously expected. Conversely, the reference source used for this off-line identification must be modeled with enough accuracy, and its design is probably more challenging than expected. Both simulations and experimental results show that it is possible to use the same microphones for off-line identification and for active control. Although this configuration does not satisfy some of the mathematical assumptions used in Ref. [28], it leads to a convenient system which requires a reasonable number of transducers, all fitted on the walls. This is therefore a significant step toward a realistic system able to extend the frequency range of small available facilities toward lower frequencies.

Further analysis is however needed to investigate the many parameters governing such a system before an optimal configuration may be proposed. A more extensive experimental validation should involve numerous sources with var-

ious radiation characteristics, helping to better understand the various phenomena which may limit the performances of such a system at higher frequencies. The controlled pressure was obtained here as a linear combination of measurements performed without control, assuming that the control sources behave linearly. This will not be possible for non-stationary sources, which will require further work. Dealing with all these pending aspects will require considering a practical situation where the surface Γ surrounds the whole measuring volume, such as a room, probably smaller, but with all its walls fitted with both passive lining and active control of scattering.

Acknowledgements

The authors wish to thank their colleagues, Régine Guillermin for a specific version of the BEM code and Fabrice Silva for fruitful discussions and his help in preparing the final manuscript. They also thank the anonymous reviewers for constructive comments which helped to improve the manuscript.

References

[1] IEC 60268-5, Sound system equipment - part 5: loudspeakers, Standard of the International Electrotechnical Commission (2007).

[2] AES 2-2012, Aes standard for acoustics - methods of measuring and specifying the performance of loudspeakers for professional applications - drive units, Standard of the Audio Engineering Society (2012).

[3] M. Melon, C. Langrenne, D. Rousseau, P. Herzog, Comparison of four subwoofer measurement techniques, J. Audio Eng. Soc. 55 (12) (2007) 1077–1091.

[4] M. Melon, C. Langrenne, P. Herzog, Evaluation of a method for the measurement of subwoofers in usual rooms, J. Acoust. Soc. Am. 127 (1) (2010) 256–263.

[5] M. Sanalatii, P. Herzog, R. Guillermin, M. Melon, N. Poulain, J.-C. Le Roux, Estimation of loudspeaker frequency response and directivity using the radiation-mode method, J. Audio Eng. Soc. 67 (3) (2019) 101–115. doi:10.17743/jaes.2019.0001.

[6] F. Olson, Harry, G. May, Everett, Electronic sound absorber, J. Acoust. Soc. Am. 25 (1953) 1130–1136. doi:10.1121/1.1907249.

[7] M. Jessel, J., G. Mangiante, Active sound absorbers in an air duct, J. Sound Vib. 23 (3) (1972) 383–390. doi:10.1016/0022-460X(72)90633-5.

[8] D. Guicking, E. Lorenz, An active sound absorber with porous plate, J. Vib. Acoust. Stress Reliab. 106 (3) (1984) 389–392. doi:10.1115/1.3269206.

[9] D. Guicking, K. Karcher, M. Rollwage, Coherent active methods for applications in rooms acoustics, J. Acoust. Soc. Am. 78 (4) (1985) 1426–1434. doi:10.1121/1.392860.

[10] F. Orduña-Bustamante, P. Nelson, An adaptive controller for the active absorption of sound, J. Acoust. Soc. Am. 91 (5) (1992) 2740–2747. doi:10.1121/1.403779.

[11] M. Furstoss, D. Thenail, M.-A. Galland, Surface impedance control for sound absorption : direct and hybrid passive-active strategies, J. Sound Vib. 203 (2) (1997) 219–236. doi:10.1006/jsvi.1996.0905.

[12] C. Guigou, R. Fuller, C., Adaptive feedforward and feedback methods for active-passive sound radiation control using smart foam, J. Acoust. Soc. Am. 104 (1) (1998) 226–231. doi:10.1121/1.423290.

[13] M. Collet, P. David, M. Berthillier, Active acoustical impedance using distributed electrodynamical transducers, J. Acoust. Soc. Am. 125 (2) (2009) 882–894. doi:10.1121/1.3026329.

[14] B. Betgen, M.-A. Galland, A new hybrid active/passive sound absorber with variable surface impedance, Mech. Syst. Sig. Proc. 25 (5) (2011) 1715–1726.

[15] P. Leroy, A. Berry, P. Herzog, N. Atalla, Experimental study of a smart foam sound absorber, J. Acoust. Soc. Am. 129 (1) (2011) 154–164. doi:10.1121/1.3514502.

[16] H. Lissek, R. Boulandet, R. Fleury, Electroacoustic absorbers: bridging the gap between shunt loudspeakers and active sound absorption, J. Acoust. Soc. Am. 129 (5) (2011) 2968–2978. doi:10.1121/1.3569707.

[17] E. Rivet, S. Karkar, H. Lissek, Multi-degree-of-freedom low-frequency electroacoustic absorbers through coupled resonators, Applied Acoustics 132 (2018) 109 – 117. doi:10.1016/j.apacoust.2017.10.019.

[18] C. L. Scandrett, Y. S. Shin, K. C. Hung, M. S. Khan, C. C. Lilian, Cancellation techniques in underwater scattering of acoustic signals, J. Sound Vib. 272 (3-5) (2004) 513–537. doi:10.1016/S0022-460X(03)00381-X.

[19] E. Friot, C. Bordier, Real-time active suppression of scattered acoustic radiation, J. Sound Vib. 278 (3) (2004) 563–580. doi:10.1016/j.jsv.2003.10.064.

[20] E. Friot, R. Guillermin, M. Winninger, Active control of scattered acoustic radiation: a real-time implementation for a three-dimensional object, Acta acustica united with acustica 92 (2006) 278–288.

[21] N. Han, X. Qiu, S. Feng, Active control of three-dimension impulsive scattered radiation based on a prediction method, Mech. Syst. Signal Process. 30 (2012) 267–273.

[22] J. Cheer, Active control of scattered acoustic fields: cancellation, reproduction and cloaking, J. Acoust. Soc. Am. 140 (3) (2016) 1502–1512.

[23] C. House, J. Cheer, S. Daley, An experimental investigation into active structural acoustic cloaking of a flexible cylinder, Applied Acoustics 170 (2020) 107436.

[24] S. J. Elliott, M. Orita, J. Cheer, Active control of the sound power scattered by a locally-reacting sphere, J. Acoust. Soc. Am. 147 (3) (2020) 1851–1862.

[25] E. Friot, Control of low-frequency wall reflections in an anechoic room, in: ACTIVE 2006, Australian Acoustical Society, Australia, 2006, pp. CD–ROM (9 pages).

[26] E. Friot, A. Gintz, Estimation and global control of noise reflections, in: Active 2009, Ottawa, Canada, 2009.

[27] P. Herzog, E. Friot, D. Habault, C. Pinhede, A. Gintz, P. Leroy, M. Pachebat, Toward an active anechoic room, in: 7th Forum Acusticum, no. R01-3, European Acoustical Association, Krakow, Poland, 2014.

[28] D. Habault, E. Friot, P. Herzog, C. Pinhède, Active control in an anechoic room : theory and first simulations, Acta Acustica united with Acustica 103 (3) (2017) 369–378. doi:10.3813/AAA.919066.

[29] C. Pinhède, D. Habault, P. Herzog, E. Friot, Contrôle actif du champ diffracté en basse fréquence dans une salle semi-anéchoïque (active control of the diffracted field at low frequency in a semi-anechoic room), in: Congrès Français d'Acoustique, Le Havre, France, 2018.

[30] S. J. Elliott, Signal processing for active control, Academic Press, San Diego, Calif. London, 2001.

[31] E. Friot, Time-domain versus frequency-domain effort weighting in active noise control design, J. Acoust. Soc. Am. 141 (1) (2017) EL11–EL15. arXiv:https://doi.org/10.1121/1.4973276, doi:10.1121/1.4973276.
URL https://doi.org/10.1121/1.4973276

[32] A. Novak, P. Lotton, L. Simon, Synchronized swept-sine: theory, application, and implementation, J. Audio Eng. Soc 63 (10) (2015) 786–798.
URL http://www.aes.org/e-lib/browse.cfm?elib=18042

[33] C. Pinhède, P. Herzog, Design and measurement of a reference source at lower frequencies, in: Forum Acusticum, Lyon, France, 2020.

[34] S. Schneider, C. Kern, Acoustical behavior of the large anechoic chamber at the laboratoire de mécanique et d'acoustique in the low frequency range, Acta Acustica united with Acustica 94 (1) (2008) 141–147.